CellPress

Current Biology

Review

Molecular mechanisms underlying microtubule growth dynamics

Joseph M. Cleary and William O. Hancock*
Department of Biomedical Engineering, Pennsylvania State University, University Park, PA 16802, USA
*Correspondence: woh1@psu.edu
https://doi.org/10.1016/j.cub.2021.02.035

SUMMARY

Microtubules are dynamic cytoskeletal filaments composed of αβ-tubulin heterodimers. Historically, the dynamics of single tubulin interactions at the growing microtubule tip have been inferred from steady-state growth kinetics. However, recent advances in the production of recombinant tubulin and in high-resolution optical and cryo-electron microscopies have opened new windows into understanding the impacts of specific intermolecular interactions during growth. The microtubule lattice is held together by lateral and longitudinal tubulin–tubulin interactions, and these interactions are in turn regulated by the GTP hydrolysis state of the tubulin heterodimer. Furthermore, tubulin can exist in either an extended or a compacted state in the lattice. Growing evidence has led to the suggestion that binding of microtubule-associated proteins (MAPs) or motors can induce changes in tubulin conformation and that this information can be communicated through the microtubule lattice. Progress in understanding how dynamic tubulin–tubulin interactions control dynamic instability has benefitted from visualizing structures of growing microtubule plus ends and through stochastic biochemical models constrained by experimental data. Here, we review recent insights into the molecular basis of microtubule growth and discuss how MAPs and regulatory proteins alter tubulin–tubulin interactions to exert their effects on microtubule growth and stability.

Introduction

Microtubules are long cytoskeletal filaments found throughout all cell types and are essential for mitosis, cell motility, and intracellular transport. They are composed of αβ-tubulin heterodimers that assemble with neighboring tubulin through the formation of lateral (side-to-side) and longitudinal (top-to-bottom) interactions, creating a hollow cylinder typically comprising 13 protofilaments[1–3] (Figure 1). Microtubules are created either through the spontaneous assembly of the αβ-tubulin heterodimer into a microtubule seed, a process known as nucleation, or through growth from a stabilized template[4–6]. Once formed, microtubules present two kinetically distinct ends known as the plus end and the minus end[7]. Since the 1980s, measuring the steady-state growth rate as a function of the free tubulin concentration has been an invaluable tool for estimating the tubulin binding kinetics that occur at the microtubule end[7,8]. In recent years, innovations in microscopy that have increased signal-to-noise ratios, together with novel tracking algorithms that allow for sub-pixel localization, have greatly improved the precision with which the tips of growing microtubule ends can be localized[9–11]. These advances provide a much more detailed view of growth dynamics, but they are still insufficient to discern the addition and loss of individual ~8 nm tubulin heterodimers at a growing end.

One of the unique characteristics of microtubules is their ability to undergo dynamic instability, a switching from growth to shrinkage (catastrophe), and from shrinkage back to growth (rescue)[12]. The addition of GTP-bound tubulin to the growing end has been proposed to act as a protective cap against catastrophe, with the onset of a catastrophe resulting from the GTPase activity of the αβ-tubulin in the lattice[13]. This 'GTP cap' model was proposed[12,14–16] and later confirmed through observation of continuous microtubule growth without catastrophe in the presence of GMPCPP, a non-hydrolyzable GTP analog[8]. By visualizing fluorescently tagged end-binding protein 1 (EB1), which binds to the GTP-like conformation of tubulin[17–19], the cap size was determined to increase proportionally with the free tubulin concentration[13,20,21]. This observation, along with the finding that the cap deteriorates immediately preceding catastrophe, supports the idea that at a growing plus end a kinetic race exists between the addition of GTP-tubulin from solution and the hydrolysis of GTP in the microtubule lattice[13,20,21].

This review focuses on microtubule growth and the tubulin–tubulin interactions that dictate the likelihood of incorporation of incoming tubulin at a growing end. Apparent on-rates and off-rates of single tubulin dimers were initially estimated by measuring the average growth rates over increasing tubulin concentrations (Figure 2B)[7]. Utilizing these growth rate data, biochemical models were developed and constrained to interpret the specific tubulin–tubulin interactions occurring at the microtubule tip[22–27]. Although these models of microtubule growth have provided invaluable insights into potential tubulin–tubulin interactions, parameters in these models can vary by orders of magnitude from one another. Fortunately, recent advances in structural and single-molecule approaches have allowed this parameter space to be narrowed considerably. Our goal in this review is to consolidate the large amount of data that has been generated in recent years through the use

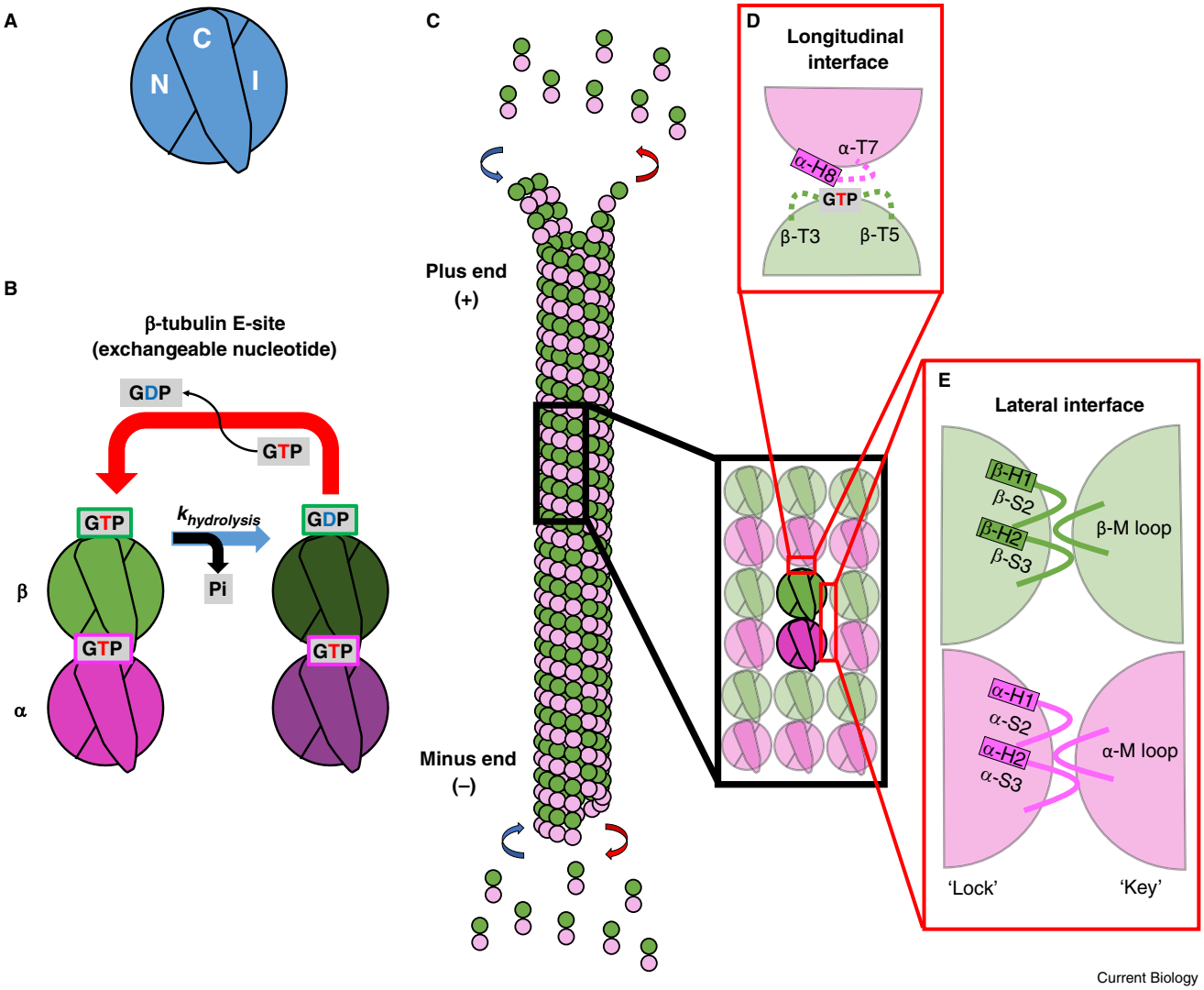

Figure 1. Domains of tubulin and the interdimer contacts involved in microtubule growth.
(A) The three domains that make up a tubulin monomer: the amino-terminal domain containing the nucleotide pocket (N), the intermediate domain made from the globular region of the protein (I), and the carboxy-terminal tail (C) facing the outside of the microtubule. (B) The exchangeable GTP-binding site (E-site), where GTP hydrolysis and nucleotide exchange occurs, is located in the N-domain of β-tubulin. Tubulin can be in either the GTP- or GDP-bound state. Meanwhile, GTP bound to the N-domain of α-tubulin has been reported to be non-exchangeable and resides in a catalytically inactive nucleotide pocket with the longitudinally bound β-tubulin. (C) Schematic of tubulin dimer dynamics at the plus and minus ends. (D) Longitudinal (top-to-bottom) dimer–dimer contacts involve interactions between the N-domain of the β-tubulin of one dimer and the I-domain of the α-tubulin of a second dimer. This longitudinal interaction between dimers forms a nucleotide pocket around the exposed GTP on the β-tubulin. (E) Lateral (side-to-side) dimer–dimer contacts form a 'lock-and-key' pocket between the I-domain of one tubulin dimer and the N-domain of the adjacent dimer.

of recombinant tubulin, single particle analysis, and improved cryo-electron microscopy (cryo-EM) resolution to move closer to a consensus model that describes the dynamic interactions that underlie microtubule growth.

Longitudinal and lateral neighbor interactions

αβ-tubulin heterodimers are formed through the dimerization of two structurally similar monomers of α- and β-tubulin. Each of these monomers is composed of three domains: the N-domain containing the nucleotide-binding pocket; the I-domain made from the primarily globular portion of the tubulin; and the C-domain that contains an unstructured, negatively charged carboxy-terminal tail that extends out from the lattice and interacts electrostatically with microtubule-associated proteins (MAPs) and microtubule motors (Figure 1A)[28–31]. Formation of a heterodimer creates an asymmetry in which an exchangeable GTP lies at the upper exposed longitudinal interface of the β-tubulin and the I-domain lies at the lower exposed longitudinal interface of the α-tubulin (Figure 1B)[32,33]. Thus, microtubules that polymerize from tubulin heterodimers are polarized filaments that present an exposed N-domain of the β-tubulin on the faster growing plus end and an exposed I-domain of the α-tubulin on the slower growing minus end (Figure 1C)[34].

In the microtubule lattice, αβ-tubulin heterodimers interact both longitudinally (head-to-tail) and laterally (side-to-side).

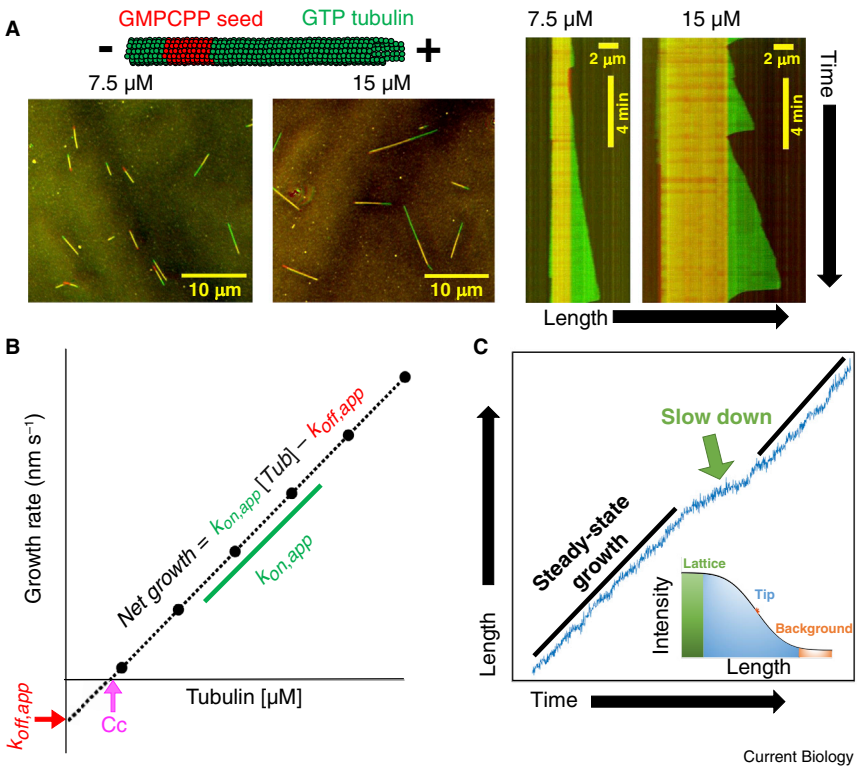

Figure 2. Experimental measurements of tubulin kinetics.
(A) Schematic of microtubule growth *in vitro* from stabilized GMPCPP seeds. Images show growth from GMPCPP seeds after a 10-minute incubation in 7.5 μM and 15 μM free tubulin. The kymographs on the right show the associated growth dynamics, which include periods of steady growth and catastrophes. (J.M.C., unpublished data.) (B) Schematic plot of the mean microtubule growth rate as a function of the free tubulin concentration. The critical concentration for growth (C_c) is estimated from the x-intercept, the apparent tubulin on-rate constant ($k_{on,app}$) is estimated from the slope, and the apparent tubulin off-rate constant ($k_{off,app}$) is estimated from the negative of the y-intercept. (C) Localization of microtubule end positions at a high spatial resolution is resolved by fitting the spatial decay of intensity using a survival function (inset) revealing fluctuations in growth and slow down events. (J.M.C., unpublished data.)

Advances in cryo-EM have enabled visualization of the specific loops and helices involved in these interactions[28,29]. Longitudinal interactions at the plus end are mediated by the βT3 and βT5 loops that surround the exposed GTP in the β-subunit, and the αT7–H8 loops in the incoming α-subunit (Figure 1D). Formation of a longitudinal interface between heterodimers brings the catalytically active Glu254 residue in the α-tubulin of the incoming heterodimer close to the β-tubulin-bound GTP of the lattice-bound heterodimer, enabling GTP hydrolysis (Figure 1B)[28,29,35–37]. Thus, an incoming tubulin must land to trigger hydrolysis of the GTP exposed at the plus end. The second nearest neighbor interaction that αβ-tubulin makes is the lateral binding interface. The most stable lateral interactions involve β–β and α–α contacts, as a B-lattice configuration[1,38]. Lateral contacts have been described as a 'lock-and-key' interaction in which the flexible M-loop, composed of the α/β S7–H9 loop in the I-domain, docks into a corresponding lock, formed from the α/β H1–S2 loop and the α/β S7–H9 loop in the N-domain, of an adjacent tubulin (Figure 1E)[28,29,39–41]. Although the microtubule lattice is predominantly in this B-lattice configuration, a shallow pitch in the lattice results in a mismatch or 'seam', generating the A-lattice configuration, in which α- and β-tubulin laterally interact[1,38]. The A-lattice seam is thought to be thermodynamically weaker based on molecular modeling and the observation that A-lattice-rich microtubules undergo catastrophe more frequently and shrink more quickly than B-lattice-rich microtubules[42]. The strength of the longitudinal and lateral interactions dictates the growth kinetics at the growing microtubule tip, and differences in these interactions upon GTP hydrolysis underlie dynamic instability.

A simple kinetic model of microtubule growth

The microtubule growth rate has been shown to vary linearly with the free tubulin concentration *in vitro*[7], providing insights into tubulin binding kinetics at the growing tip (Figure 2). The growth rate reflects a balance of tubulin association and dissociation; thus, in a plot of the growth rate versus the free tubulin concentration (Figure 2B), the apparent tubulin on-rate constant is given by the slope, and the apparent tubulin off-rate is given by the negative y-intercept. Regulation of microtubule growth by regulatory proteins or other perturbations can be described by modulation of these apparent rate constants; however, these apparent rates do not describe with molecular detail the specific tubulin–tubulin interactions occurring at the microtubule tip. Determining the true intermolecular on- and off-rates at the tip requires quantitative models that are constrained by the experimental data, and there is a rich literature of models that have evolved in parallel with experimental advances[22–25,43–45]. The simplest model to describe microtubule growth utilizes three parameters: the bimolecular on-rate constant, the longitudinal bond strength, and the lateral bond strength. The model developed by VanBuren *et al.*[22] was the first to be trained against comprehensive measurements of microtubule dynamics, and it has been applied widely to interpret quantitative experiments[22,24–26,45,46]. Despite its apparent simplicity, this model captures much of the complexity of microtubule growth and is an excellent tool for framing many of the current questions in the field.

In this simple kinetic model (Figure 3), the kinetics of tubulin–tubulin interactions are dictated by their binding free energy, where the binding affinity (K_a) increases exponentially with the total free energy of interaction, $K_a = \frac{k_{on}}{k_{off}} = e^{-\frac{\Sigma\Delta G_{long} + \Sigma\Delta G_{lat}}{k_B T}}$. This relationship makes it especially important to understand the energetic contributions of each of the lateral and longitudinal interactions occurring at the growing microtubule tip. Because lateral interactions are thought to be weaker than longitudinal

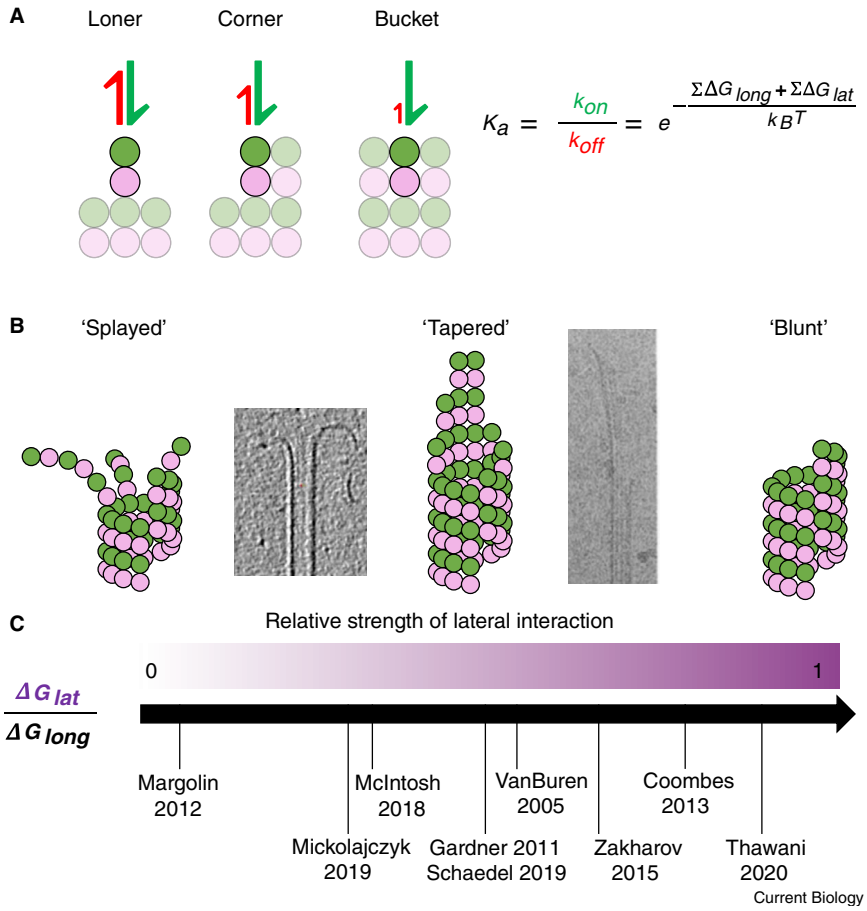

Figure 3. A simple model of microtubule growth.
(A) The affinity of loner, corner, and bucket sites at the growing plus end are exponential functions of the free energy of the underlying lateral and longitudinal contacts (based on VanBuren *et al.*[22]). (B) As the relative free energies of lateral to longitudinal bonds increases, the growth dynamics transition from 'splayed', where protofilaments grow relatively independently, to 'tapered', where incorporation predominantly occurs at corner sites, to 'blunt' or 'barber pole', where the weak longitudinal bond dictates that growth occurs only from corner sites. Accompanying cryoEM images display a splayed end (© 2018 J. Cell Biol., originally published in McIntosh *et al.*[70]) and a tapered end (© 1995 J. Cell Biol., originally published in Chrétien *et al.*[51]). (C) Different microtubule growth models in the field incorporate very different values for the relative free energy of lateral and longitudinal bonds. Specific parameter values for the different models are presented in Table 1.

interactions, single lateral bonds are generally not considered. Thus, the simplest interaction, and the one with the highest likelihood of reversibility, is the 'loner' interaction consisting of one longitudinal interface[22,40] (Figure 3A). Adding one lateral neighbor creates a 'corner' interaction that is exponentially stronger and thus has a much lower likelihood of detachment of the incoming tubulin dimer. The addition of a second lateral neighbor results in a 'bucket' configuration, which has the highest interaction energy and lowest likelihood of detachment of the incoming tubulin dimer from the microtubule tip. Finally, if a second longitudinal neighbor is added to surround a tubulin on all four sides, then that subunit is assumed to be tightly but reversibly incorporated into the lattice[45–48]. When these simple kinetic rules are combined with a tubulin binding rate that is proportional to the free tubulin concentration, the growth of the 13 protofilaments in the lattice can be simulated to gain insights into microtubule growth. Because an incoming tubulin dimer interacts with loner, corner, and bucket configurations with such different interaction energies, the shape of the taper at the plus end, which determines the proportion of different binding events, strongly affects the growth dynamics[22,24,45].

Although these fundamental kinetic principles are generally agreed upon, experimental steady-state growth rate data are not sufficient to constrain the model parameter values. The result, as shown in Table 1, is that a number of models exist in the literature that can reproduce the experimental growth data whilst employing vastly different parameters. More importantly, the different models imply different mechanisms of growth and predict qualitatively different microtubule tip structures (Figure 3B)[45]. To develop intuition about how relative longitudinal and lateral binding free energies lead to different mechanisms of growth, we outline below a simple biochemical model where the corner affinity, defined by the free energy of one lateral plus one longitudinal bond, is held constant. It has been shown that the tubulin on-rate constant and the relative lateral and longitudinal free energies can be varied while still recapitulating the experimental growth curve shown in Figure 2B [22,49,50]. Varying the relative strengths of the lateral and longitudinal bonds results in three different 'modes' of microtubule growth (depicted in Figure 3B).

In the 'splayed' model, if growth involves strong longitudinal bonds and weak lateral bonds, growth is dominated by loner interactions, resulting in independently elongating protofilaments at the microtubule end. Continuous growth in this model depends on the rate of lateral bond formation between protofilaments that close the microtubule into a cylinder. In this scenario, the tubulin on-rate constant would need to be relatively slow because loners that make only one longitudinal interaction have a relatively high probability of being incorporated into the growing protofilament.

In the 'tapered' model, as the lateral affinity is dialed up, with a compensatory decrease in the longitudinal affinity, the microtubule is predicted to grow with a sheet-like taper at its tip. Tapered growth results from an increased importance of corner interactions, since loners tend to dissociate before being incorporated. Because of this rapid dissociation of loners, a compensatory increase in the tubulin on-rate constant is required to match steady-state growth rates. Though loner dissociation rates are higher, the increased on-rate increases the likelihood of the association of a neighboring tubulin trapping it in a corner interaction.

Table 1. Model parameters of prominent biochemical and chemomechanical models of microtubule growth.

Paper	k_{on} (μM^{-1} s^{-1} pf^{-1})	ΔG_{long} (k_BT)	ΔG_{lat} (k_BT)	Loner dwell time (ms)	Corner dwell time (ms)
Biochemical models					
Mickolajczyk *et al.*[45]	0.8 (yeast)	–12	–3.6	203.4	7445.7
Schaedel *et al.*[46]	1	–18.8	–9.4	0.1[a]	984.6[a]
Margolin *et al.*[112]	1.25	–9.4	–0.3	9.7	13.1
Thawani *et al.*[60]	1.3	–7.2	–6.5	1	685.3
VanBuren *et al.*[22]	2	–9.4	–3.2	6	148.3
	4	–6.8	–5.7	0.2	67.1
Piedra *et al.*[26]	4 (yeast)	–5.8	–6.6	0.1	60.7
Gardner *et al.*[24]	4	–9.5	–5	3.3	495.7
Coombes *et al.*[52]	5	–7.2	–5.7	0.3	80.1
Chaaban *et al.*[41]	6 (*C. elegans*)	–7.1	–6.4	0.2	121.6
	6	–6.3	–5	0.1	13.5
Chemomechanical models					
Zakharov *et al.*[25]	0.63	–15.5	–9.1	N/A	N/A
McIntosh *et al.*[70]	0.63	–16.6	–5.3	N/A	N/A
Gudimchuk *et al.*[43]	0.63	–16.9	–13.5	N/A	N/A
Castle *et al.*[63]	12.7 (loner)	–6.7	N/A	0.1[a]	N/A
	7.4 (corner)	–6.7	–3.6	N/A	4[a]

Dwell times are calculated by using free energy to solve for the equilibrium constant, using the on-rate to calculate the off-rate, and inverting the off-rate. Dwell times denoted as 'N/A' were not calculated for chemomechanical models where entropic penalties were not specifically stated.
[a]Includes entropic penalty specified in the paper.

In the 'blunt' model, if the longitudinal affinity is further weakened to a point where it matches the lateral bond affinity, then the probability of loners incorporating is negligible and microtubule growth will occur solely through corner interactions. The result is that the microtubule grows in a spiral 'barber pole' fashion, with a blunt microtubule tip. The tubulin on-rate constant in this case would need to be sufficiently high that there is a high likelihood of two tubulin dimers landing in adjacent protofilaments before detaching from the microtubule end. In this model, growth of a new ring of tubulin could also start at the seam, where there will always be a half-heterodimer offset.

The structure of the growing microtubule tip and the specific parameter values for the on-rate constant and the longitudinal and lateral affinities are hotly debated in the field (Figure 3C and Table 1). Below, we describe the experimental evidence and the kinetic and thermodynamic arguments for each of these models.

Microtubule end structures

Tapered microtubules

Microtubule tapers, which provide a range of possible binding configurations for incoming tubulin, are the most widely supported model for the tips of growing microtubules. Microtubule tapers were first visualized by electron microscopy as long, gradually curved, sheet-like structures projecting from the ends of growing microtubules[51]. Further evidence for tapered plus ends came from fluorescence imaging, with the challenge being the inherent blurring of ends by the point spread function of the microscope. By performing model convolution on simulated images, the predicted spatial decay of fluorescence at the microtubule tip for different tip taper lengths can be predicted and used to infer tip structure[52,53]. Using this approach, Coombes *et al.*[52] presented evidence that the taper evolves during microtubule growth from a seed and reaches a steady-state length that varies with the free tubulin concentration. This approach has been extended to show that microtubule plus tips are elongated in cells and when microtubules are grown *in vitro* in the presence of regulatory proteins[11,54,55]. However, using similar approaches, Maurer *et al.*[20] concluded that taper lengths for microtubules grown under standard conditions *in vitro* were below the detection limit of ~180 nm for this technique, which they established using model convolution. These conflicting results may arise from differences in tubulin-labeling ratios, signal-to-noise ratios of the imaging systems, or averaging techniques used to fit the microtubule end. Label-free approaches such as interference reflection and interferometric scattering microscopy[56–58], where the scattering intensity is proportional to the mass of protein present, may provide greater precision into measuring taper lengths below the optical limit.

A third line of evidence in support of the tapered model of growth comes from the kinetics of templated nucleation, in which microtubules are grown from blunt GMPCPP-stabilized seeds. Wieczorek and colleagues[59] observed that near the critical concentration for growth (C_c at the x-intercept in Figure 2B) there was no measurable growth from blunt-tipped GMPCPP seed microtubules. Although growth from seeds near the C_c has been observed under some conditions[60], this result is also consistent with the relatively low number of seeds that have plus-end extensions at moderate tubulin concentrations[54,59]. One explanation is that, because loners rarely incorporate on a blunt end, there is a kinetic battle to establish sufficient corner sites to enable steady microtubule growth. This model was

tested by exposing microtubule seeds to a high concentration of free tubulin that allowed for the formation of a tapered template, and then dropping the tubulin concentration close to the C_c where growth was previously not observed. Growth rates following this 'priming' matched the predicted steady-state growth at the lower tubulin concentration (e.g. Figure 2B), consistent with formation of a tapered tip being a prerequisite for steady-state growth. At this point, evidence for tapered microtubule plus ends is sufficiently widespread that the possibility that growing microtubule ends are blunt is no longer considered in the field. However, the tapered model of microtubule growth leaves a wide parameter space for the on-rate constant and lateral and longitudinal bond strengths. Fortunately, these tapered tip models can be split into two camps: a fast-kinetics model in which the longitudinal affinity is relatively low and the on-rate high to compensate[24], and a slow-kinetics model in which the longitudinal bond strength is relatively strong and growth is achieved by a moderate bimolecular on-rate for tubulin addition to a growing protofilament[45].

Tubulin addition can be described as either efficient, meaning that most tubulin that land are incorporated, or inefficient, where only a small fraction contribute to growth as a result of their rapid dissociation. Based on this reasoning, Gardner and colleagues[24] created an analytical model coupled with simulations to show that these two scenarios predict very different fluctuation behavior of the growing microtubule tip. Growing microtubule plus tips were then tracked by high-precision fluorescence microscopy in the presence of both GMPCPP and GTP. The large amplitude length fluctuations observed were consistent with an inefficient model of growth, in which tubulin on- and off-rates are considerably faster than previously reported (Figure 2B)[21,24]. These observations were supported by optical trapping experiments in which microtubules were grown against a barrier and rapid fluctuations with amplitudes matching single tubulin dimers or tubulin oligomers were detected[61,62]. In the simple kinetic model in Figure 3, the fast-kinetics model would correspond to a weak longitudinal affinity with tubulin addition occurring almost exclusively through corner interactions in a barber-pole fashion[45]. However, the authors were able to measure relatively large tapers based on fluorescent images at the growing plus end[24]. This was reconciled by positing an on-rate penalty based on the structure of the binding site: loners land with a fast on-rate, binding into corners occurs somewhat more slowly, and the on-rate for bucket sites is an order of magnitude slower[24]. Support for the penalty was provided using Brownian dynamics simulations, arguing that constraints from lateral neighbors suppress the on-rate[63]. This on-rate penalty, which is physically reasonable but difficult to experimentally verify, creates a positive feedback loop in which lagging protofilaments grow even more slowly while longer protofilaments grow at normal rates, generating a large taper over time. One appealing feature of this fast-kinetics model is that it provides a simple explanation for how diverse regulatory proteins can alter microtubule growth rates: if the on- and off-rates are fast and the difference between them is small, then small variations in these fast rate constants can produce large changes in the net growth rate[24].

One reason that numerous models for microtubule growth exist in the field is that there are a range of reasonable assumptions that can be made that result in quite different mechanisms of growth. Therefore, without the ability to measure the kinetics of single tubulin dimers directly, it is difficult to limit the range of bond strengths and on-rates used to model microtubule growth. This situation was addressed recently by Mickolajczyk and coworkers[45], who used interferometric scattering (iSCAT) microscopy to measure the reversible binding of gold nanoparticle-labeled tubulin at growing microtubule plus ends. This work employed recombinant yeast tubulin that was labeled at its carboxyl terminus with a 20 nm gold particle, and microtubules grown from immobilized axonemes (the microtubule-based core of a cilium or flagellum) in the presence of GTPγS, a slowly hydrolyzable GTP analog. The gold decreased the diffusion constant of the tubulin by approximately threefold, but control experiments showed that the labeling did not alter the ability of tubulin to be incorporated into the lattice. When gold-labeled tubulin was visualized at the growing plus end in the presence of a ~1,000-fold excess of unlabeled tubulin, three types of events were observed: incorporation into the lattice; reversible binding with a long dwell time (~1 s); and reversible binding with a short dwell time (~30 ms). These results were consistent with expectations if the incoming tubulin binds to a tapered microtubule tip, but it left open the question of whether fast and slow events corresponded to loners and corners, respectively, or corners and buckets, respectively, with the loner events being too fast to measure in the latter (Figure 3A). This uncertainty was resolved using mutants with altered lateral or longitudinal interfaces, and modeling the results using a computational model similar to that shown in Figure 3 [45,64,65]. The conclusion was that the fast events reflected loners, the slow events were corners, and the irreversible events were bucket sites. The data were best fit by a model in which the on-rate was constant for all binding sites at 10 μM^{-1} s^{-1} tip^{-1}, roughly sixfold slower than the fast-kinetics model[24].

Thus, the fast-kinetics and slow-kinetics models are able to match experimental tubulin-dependent growth rates and predict a tapered plus end by slightly different mechanisms. The fast-kinetics model of Gardner and colleagues[24] generates a tapered tip using the added feature of a slow on-rate to bucket sites, whereas the iSCAT work of Mickolajczyk and coworkers[45] achieves a tapered tip because the slower dissociation rate of loners enables more corner interactions to occur. As detailed in Table 1, fast-kinetics models incorporate a very low loner affinity and slow-kinetics models have a moderate loner affinity. Expanding the picture, a third class of models that model the plus end as a splayed structure incorporate even higher loner affinities.

Are growing microtubule ends splayed?

Early electron microscopy revealed curved protofilaments, commonly referred to as ram's horns, present at the tips of depolymerizing microtubules[66]. This finding, along with our understanding of the role of hydrolysis in microtubule catastrophe, led to the textbook model in which GTP-bound tubulin was in a straight conformation, while GDP-bound tubulin was in a curved conformation[67]. This model was invalidated, however, by the finding that isolated tubulin is curved in both GTP- and GDP-bound states[68,69]. Adding to this picture, recent work using cryo-electron tomography (cryo-ET) captured curved protofilaments at the growing plus ends of microtubules, and described

growing plus ends as 'flared' or 'splayed'[70]. The splayed protofilaments were measured to be around two to four tubulin dimers in length and had curvatures of 12–20°, nearly matching the curvature measured from the depolymerizing ram's horns[70]. The presence of these plus-end protofilament curls argues for a model in which longitudinal interactions are the dominant stabilizing feature during growth (Figure 3B). This model has led to a fair degree of controversy in the field, as it challenges the textbook model of a tapered microtubule end. The methodological difference in this study lay in the analysis of the tilt series. In this study, images of the microtubule end were segmented and aligned with the center of the microtubule positioned along the y-axis. Slices of the microtubule were then generated by rotary sectioning through the center of the microtubule. The standard approach uses axial sectioning, in which the slices are generated parallel to the microtubule axis, thus passing through the center in only one slice[71–73]. The advantage of the rotary sectioning is that it maximizes the signal-to-noise ratio of the rendered microtubule tip, a necessary aid in a technique that has a low signal-to-noise ratio. The disadvantage is that, because the microtubule tip is a notoriously difficult structure to image using standard electron microscopy techniques due to its heterogeneity, all the structures measured in this study required tracing by hand, making it a cumbersome process and one that requires a highly trained eye[70,74,75].

Supporting these experimental data, a detailed computational model that incorporates splayed protofilaments into the microtubule assembly process was shown to reproduce experimentally observed growth rates[43]. This chemomechanical model proposes that protofilament stiffness allows for fast fluctuations that increase the likelihood of forming weak lateral interactions that seal the splayed protofilament into the lattice. Notably, the recapitulation of experimental growth dynamics required using a fairly low tubulin on-rate, which, together with the relatively high longitudinal affinity, means that a large fraction of the tubulin that binds to the end of protofilaments is incorporated into the growing lattice (an efficient mechanism). These strong longitudinal interactions resemble another efficient model of polymer growth, that of bacterial tubulin, FtsZ[76]: in the case of FtsZ, there is a transition from a weak-binding conformation found in solution, to a strong-binding conformation that is favored when subunits are incorporated into a growing filament. These conflicting views of the structure of growing microtubule tips will likely persist for a time due to the challenge of imaging these heterogeneous, dynamic structures with high resolution. However, in parallel with continuing advances in cryo-EM imaging, additional lines of evidence are being pursued to reconcile the splayed and tapered models. Resolving this structural question will help to more quantitatively define the relative magnitudes of the longitudinal and lateral bonds that stabilize the microtubule lattice.

The curved-to-straight transition

Up to this point, we have primarily focused on the longitudinal and lateral interactions that stabilize GTP-tubulin in the lattice and have neglected details of the mechanical straightening that is required for curved tubulins in solution to become incorporated into the straight microtubule lattice. At the tip of a growing microtubule, there is a competition between the elastic bending of the dimer that favors the curved conformation, and lateral bond formation that locks tubulin in a straight conformation. Models that predict a tapered tip (e.g. Figure 3) generally account for the elastic energy involved in straightening as a penalty against lateral binding energy that stabilizes tubulin in the lattice[23]. Models incorporating splayed ends generally consider the protofilament bending flexibility, the thermal fluctuations that drive protofilament bending, and the activation energy for forming a lateral bond in greater detail, which allows for much richer behavior in the simulations but which also introduces additional free parameters[25,43]. The straightening process in these Brownian dynamics models is a form of a thermal ratchet, where the protofilaments sample many different curvatures due to thermal fluctuations and become captured in the straight conformation when a lateral bond is formed with a neighboring protofilament. The relative kinetics of tubulin straightening, lateral bond formation, and tubulin dissociation from the end of a protofilament likely play an important role in determining the growth rate and concentration dependence of growth and catastrophe.

Where does GTP hydrolysis exert its influence?

Early models of tubulin association were based on the nucleotide state of the incoming tubulin, where GTP-bound tubulin had a higher affinity for the lattice than GDP-bound tubulin[77]. This can be termed a '*cis*-acting' model, in which the nucleotide state of an incoming tubulin is what determines its affinity for the microtubule tip[67,78] (Figure 4A). However, once structures of soluble GTP- and GDP-bound tubulin were resolved to have no inherent curvature differences[69], this model lost some of its momentum because, for the nucleotide state of an incoming tubulin to determine its binding affinity in the absence of curvature differences, it would require a long-distance allosteric communication from the nucleotide pocket of the β-tubulin to the distal longitudinal interfaces of the α-tubulin that interact with the lattice. In contrast, a '*trans*-acting' model (Figure 4A) proposes that the nucleotide state of the terminal exposed β-tubulin at the microtubule plus end dictates the affinity of an incoming tubulin from solution[26,44,69]. Thus, structural rearrangements upon GTP hydrolysis would only need to occur around the nucleotide-binding pocket, which lies at the longitudinal interface between tubulin subunits. Furthermore, structural studies provide a plausible mechanism for how the nucleotide in the terminal β-subunit may regulate binding of the incoming tubulin. It was shown that the βT5 loop, which resides at the α–β interdimer interface, changes its conformation based on the identity of the bound nucleotide[68,79]. When GTP is bound, the loop flips 'out', exposing Asp177 and increasing the longitudinal interface interacting with the incoming α-tubulin. Meanwhile, when GDP is bound, the βT5 loop is able to flip 'in', resulting in a decrease in the longitudinal bond strength and faster dissociation of the terminal tubulin[68,80].

The *trans*-acting model[26] involves a kinetic race at the growing microtubule plus end that may clarify some unexplained aspects of microtubule growth in the literature. This race results from the GTP hydrolysis state of the penultimate tubulin in the lattice determining the affinity of the newly added tubulin at the plus end, and the requirement of a newly added subunit to trigger GTP hydrolysis in the lattice-bound tubulin. If hydrolysis occurs rapidly upon addition of a new tubulin, this newcomer may dissociate, which then exposes a lattice-bound GDP-tubulin at the

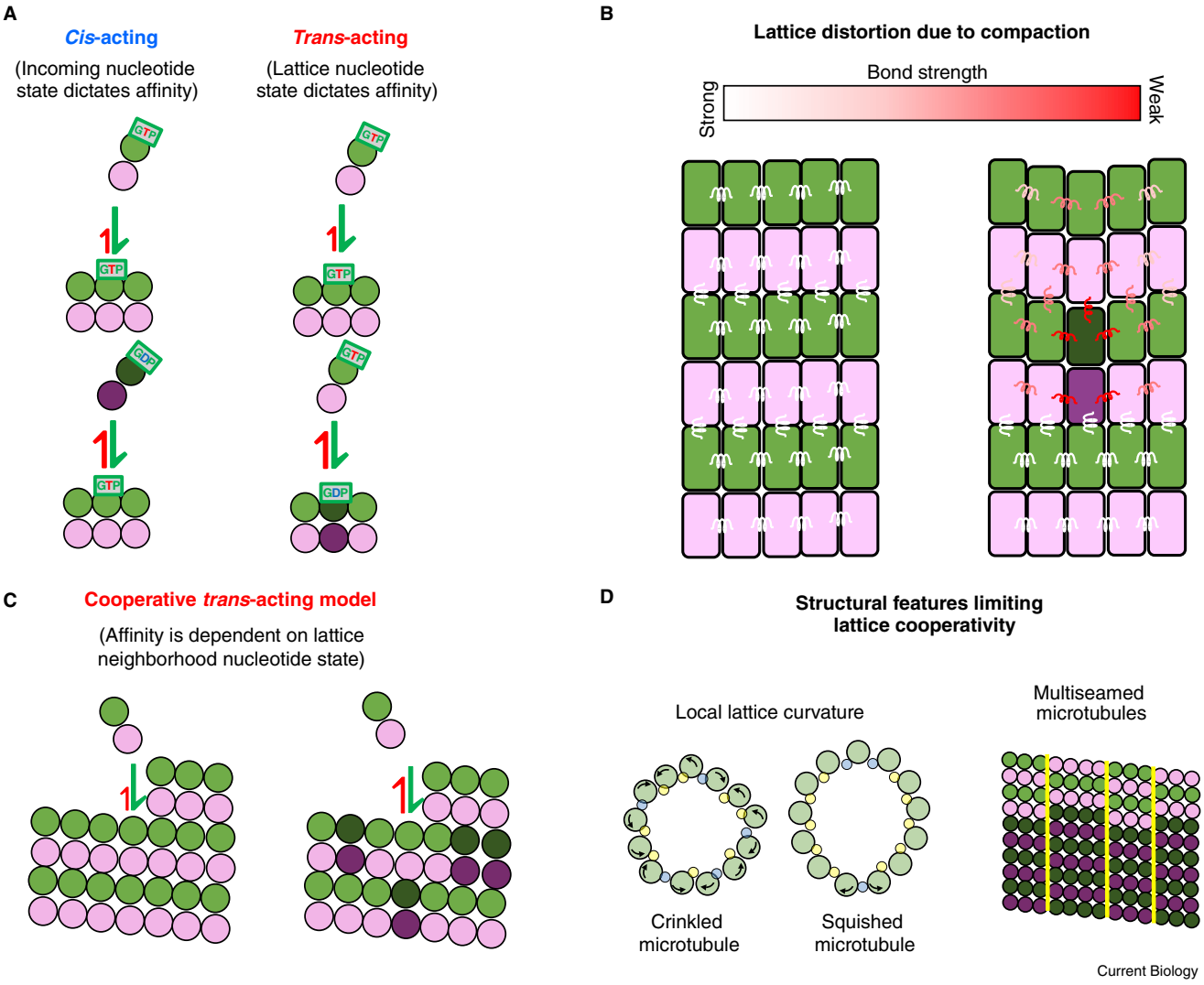

Figure 4. *Trans*-acting model of growth and lattice cooperativity.
(A) The *cis*-acting model proposes that the nucleotide state of the incoming tubulin dimer dictates binding affinity. The *trans*-acting model proposes that the nucleotide state of the terminal lattice-bound tubulin dictates binding affinity. Light and dark shading represent GTP- and GDP-bound tubulin dimers, respectively. (B) The effect of a single tubulin dimer's compaction not only has the potential to change the bond strength of nearest neighbors but also can be spread through accommodation within the lattice. (C) The cooperative *trans*-acting model proposes that the nucleotide states of neighboring tubulin in the lattice dictate the binding affinity of the incoming tubulin dimer[44]. (D) Structural features may limit the propagation of cooperative binding effects through the lattice. Local curvature changes in 'crinkled' or 'squished' microtubule lattices (left) and multiple seams (right, with the seams denoted in yellow) might limit the size of the neighborhood over which cooperative effects might act. Images of deformed microtubules based on Debs *et al.*[91].

plus end. Any tubulin subsequently added to this protofilament would then be at a disadvantage of incorporating, due to the lower binding affinity. This phenomenon may account for the unexplained increased growth rates of GMPCPP- compared with GTP-tubulin[8,81]. When first observed, this twofold difference in the apparent on-rate was thought to be insignificant and perhaps due to the modified nucleotide. However, in a recent study a hydrolysis-resistant tubulin was created by mutating α-tubulin Glu254, the residue found at the inter-tubulin longitudinal interface believed to be responsible for forming a catalytically active nucleotide pocket[82]. Along with the expected resistance to catastrophe, this mutant also grew twofold faster than wild-type tubulin under similar conditions. The fact that two different perturbations that prevent the creation of exposed GDP-tubulin at the plus end both show faster growth rates lends support to the *trans*-acting model. Additionally, during steady microtubule growth in the presence of GTP, transient pauses and slowing have been observed[13,20,83] (Figure 2C), which also may be explained by the exposed GDP-tubulin at the plus end slowing the incorporation of incoming tubulin[21,23,82,84].

Another feature that may prove useful in understanding the *trans*-acting model is the microtubule minus end. At the minus end, the terminal tubulin has its exchangeable nucleotide buried in the lattice and the incoming tubulin arrives with its exchangeable nucleotide exposed. Thus, GTP hydrolysis in the lattice may have different effects on incoming tubulin. Relevant to this,

Strothman *et al.*[85] recently showed that, compared with the plus end, minus ends have a three–fourfold slower apparent on-rate and a compensatory threefold slower off-rate, but have similar growth lifetimes preceding catastrophe. This suggests that the relationship between GTP cap size and catastrophe frequency is different at the two ends. The minus end is greatly understudied compared with the plus end, but any unified model of microtubule dynamics should be able to describe why the structural differences between the plus and minus end lead to their different polymerization dynamics.

Lattice compaction and structural plasticity

As first reported around 25 years ago[86], tubulin in the lattice of microtubules polymerized in the presence of GMPCPP is roughly 2 Å longer than tubulin in a GDP lattice. The structural disparity between these two tubulin conformations suggests that microtubules may switch their lattice states in a concerted way. This phenomenon was revisited more recently using cryo-EM, where it was found that both subunits of tubulin undergo compaction that is correlated with the nucleotide state of the lattice[29], and that compaction results in a smaller lateral contact interface and a greater longitudinal contact interface between neighboring tubulin[28]. This structural transition offers a potential mechanism for the formation of ram's horns during depolymerization: protofilaments in a compacted lattice peel away more easily from their lateral neighbors due to weakened lateral contacts but stay intact due to strengthened longitudinal contacts[28]. Complicating matters somewhat, recent work has suggested that there is not a tight correlation between the nucleotide state and the compaction state of tubulin. First, MAPs such as kinesin and EB3 have been shown to alter the compaction state of the tubulin[87–89]. Secondly, it was shown that the GDP analog GMPCP was able to expand the lattice despite lacking a terminal phosphate; it was suggested that the methylene group rather than the terminal phosphate may be driving the lattice expansion in GMPCPP microtubules[80]. Thus, it is clear that the microtubule lattice can exist in either compacted or expanded states, but the mechanisms affecting the expansion/compaction state of the lattice are an active current area of investigation.

The bistability of lattice expansion also leads to a number of questions related to structural communication through the lattice[90]. For instance, compaction of a single tubulin dimer within the lattice is expected to cause compensatory strain within the lattice to accommodate the defect. This strain may spread some distance through the lattice, and one way to relieve this strain is for the surrounding lattice to switch its compaction state. This opens up the possibility that a protein binding to one tubulin dimer may result in the alteration of the structure of neighboring tubulin dimers in the lattice. This lattice cooperativity was reported in a recent study that used kinesin to expand the lattice and found that only ~20% occupancy by kinesin was sufficient for full lattice expansion[88]. These cooperative interactions have been incorporated into detailed chemomechanical models in which tubulin–tubulin contacts are modeled as spring-like interactions that allow for energy dissipation across neighboring tubulin in the lattice[25,43] (Figure 4B). Coupled lattice interactions have also been incorporated into simpler biochemical models in which hydrolysis impacts the affinity of neighboring tubulin within a ring that is one tubulin dimer deep[44] (Figure 4C). Even this fairly minor addition significantly improved the prediction of catastrophe events. Although to date these models have been primarily applied to understanding catastrophe, implementing their principles to study microtubule growth could lead to new testable predictions regarding growth fluctuations and microtubule tip structure.

If structural transitions can propagate some distance through the lattice, what limits the distance across which these structural changes can be communicated? One limit may be the microtubule seam, where the standard B lattice involving β–β and α–α lateral interactions is interrupted by an A-lattice seam containing β–α and α–β lateral interfaces[38]. A recent cryo-EM study that used enhanced refinement algorithms to study lattice structure found that, although the lattices studied mostly contained only one seam, multiseamed microtubules are common (Figure 4D, right)[91]. The addition of multiple seams creates smaller neighborhoods of contiguous B lattice that may limit the extent of cooperative communication. Both the size of the offset between tubulin dimers found at the microtubule seam and the protofilament number have been shown to vary along individual microtubules[92] and could serve as limits for communication along the microtubule axis. These different lattice configurations lead to different protofilament skew angles and potentially different degrees of lattice strain in different regions of the lattice[93]. A recent study also showed that microtubules displayed regions of local distortion, resulting in lattice structures that were either 'squished' or 'crinkled' (Figure 4D, left)[91]. The distortions stemmed from changes in inter-protofilament curvature accommodated by a different hinge configuration of the M-loop, which is the driver of lateral interactions. These lattice deformations alter lateral contacts and provide a potential mechanism for lattice defects. Thus, the microtubule lattice is far from a static and regular structure. This structural plasticity has the benefit of allowing for different conformational states of tubulin, but it also puts potential constraints on the extent of cooperative communication through the lattice.

Cellular mechanisms for regulating microtubule growth

Most studies designed to understand the biochemical principles that underlie microtubule growth are carried out in controlled *in vitro* environments using purified tubulin. In contrast, the intracellular environment contains numerous regulatory proteins that alter microtubule structure and dynamics. One class of these is tip-trackers (Figure 5A, top), which interact with microtubule plus or minus ends and alter polymerization rates and/or catastrophe frequencies[94]. A more detailed understanding of mechanisms underlying microtubule growth should provide a framework for understanding how these regulatory proteins achieve their functions. Conversely, studying how these regulators exert their actions can provide new insights into fundamental aspects of microtubule growth and depolymerization. End-binding proteins can exert effect through lattice compaction[73], capping of microtubule ends[71,95,96], promoting the curved-to-straight transition of tubulin at the tip[11,54,97], and by shuttling tubulin along the lattice to increase the local tubulin concentration at the growing tip[98].

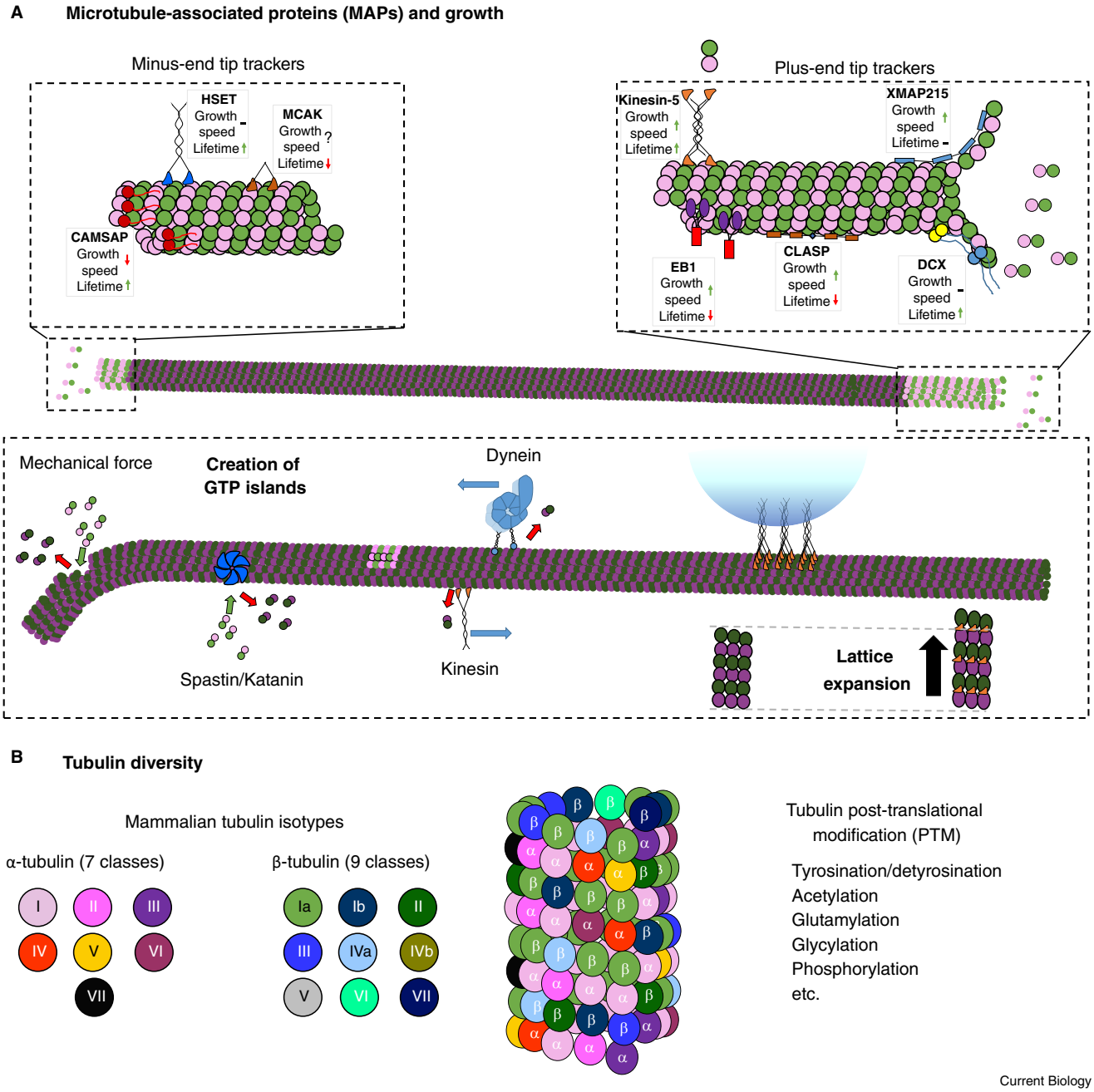

Figure 5. Cellular mechanisms for regulating microtubule growth.
(A) Microtubule-associated proteins (MAPs) that alter microtubule dynamics. Tip-tracking proteins (top) can be specific to either the plus or the minus end and can alter either microtubule growth speeds or microtubule growth lifetimes, or both (the effects are denoted by the symbols). Motors and microtubule-severing enzymes (bottom) can enhance lattice turnover and enable the formation of GTP islands. Motor binding can also drive expansion of the lattice. (B) Mammalian microtubules are formed from a number of different α- and β-tubulin isotypes, creating a mosaic microtubule lattice. Each isotype has its own unique impact on the structure, kinetics, and stability of the microtubule. Each tubulin isotype can be post-translationally modified, which can influence microtubule structure and dynamics.

In addition to exerting their influence at microtubule ends, regulatory proteins can also affect microtubule structure and dynamics through interactions with the microtubule lattice. Tubulin subunits can be removed from the lattice by physical perturbations, such as bending[46–48], or by chemomechanical forces exerted by microtubule-severing proteins such as spastin and katanin[99–102]. It was also recently shown that kinesin and dynein motors can exert sufficient force perpendicular to the microtubule wall to extract tubulin from the lattice[103]. While extracting tubulin from the lattice can lead to microtubule breakage or depolymerization, it also allows for the incorporation of new GTP-tubulin into the lattice to create 'GTP islands' that can serve

as sites where rescues occur during microtubule depolymerization[101,104,105]. The mechanical forces and thermodynamics of how these proteins extract tubulin from the lattice are still being worked out, but this work has led to a new appreciation of microtubules as dynamic structures that are continually turning over and being remodeled not only at their ends but throughout the lattice.

Most cells contain multiple isotypes of both α- and β-tubulin that dimerize to generate a range of heterodimers[106] (Figure 5), and isotype expression levels vary with cell type, resulting in cell-specific microtubule dynamics[107]. Accordingly, the brain-derived bovine or porcine tubulin used in most *in vitro* studies of microtubule dynamics contains a heterogeneous mixture of tubulin isotypes with diverse post-translational modifications. With recent breakthroughs in producing recombinant tubulin, it has become possible to uncover the functional impact of tubulin isotypes on microtubule dynamics[39,45,82,108]. Along with functional assessments, single-isotype microtubules are being used to understand the structural differences that may be guiding these functional differences. Additionally, isotype-specific post-translational modifications, such as detyrosination, glutamylation, and acetylation, may alter the structural interactions between tubulin as well as their dynamic properties[109]. This diversity opens up a number of possible mechanisms by which microtubule dynamics can be altered over time, over space, and across cell types, a system referred to as the 'tubulin code'[110,111].

Conclusions

In recent years, the microtubule field has employed recombinant tubulin, advanced single-molecule techniques, and cutting-edge structural studies to rapidly expand our understanding of the kinetics of single tubulin dimer interactions at growing microtubule tips. Despite this progress, the ultimate goal of connecting the mechanics and biochemistry of tubulin still lies in the future and will require ongoing work on multiple fronts. As described here, there are very fundamental aspects of microtubule structure and growth that are hotly debated in the field. These include the magnitudes of the on- and off-rate constants for tubulin association at the growing plus end, the relative magnitudes of lateral and longitudinal bond free energies that stabilize tubulin in the lattice, and the mechanical work necessary to straighten tubulin in different nucleotide states. The precise shape of the growing microtubule tip, from blunt to tapered to splayed, is a manifestation of these different variables; thus, defining the plus and minus tip structures under various conditions is a high-priority pursuit. Even more tantalizing is the emerging appreciation of the structural plasticity of the microtubule lattice, which brings up the possibility that binding of proteins to the lattice can alter the structure and properties of the microtubule some distance away from the binding site. Thus, microtubules could provide a mode of mid- to long-distance communication in cells. It is an exciting time in the microtubule field, and the advances on the biophysics and biochemistry of microtubule growth should lead to new paradigms with which to interpret cellular mechanisms of the regulation of microtubule dynamics as well as new perspectives for considering the impacts of tubulin diversity on microtubule function.

ACKNOWLEDGEMENTS

This work was funded by NIH R01 GM135565 and by NIH T32 GM108563. The authors thank Luke Rice (UTSW) for invaluable intellectual contributions to many of the ideas presented here, and Tae Kim and Keith J. Mickolajczyk for modeling and experimental work, respectively. The authors also thank the Hancock lab for helpful suggestions and the M4 gang for continuing enthusiasm about all things related to microtubules.

DECLARATION OF INTERESTS

The authors declare no competing interests.

REFERENCES

1. Mandelkow, E.M., Schultheiss, R., Rapp, R., and Müller, M. (1986). On the surface lattice of microtubules: helix starts, protofilament number, seam, and handedness. J. Cell Biol. *102*, 1067–1073.
2. Burton, P.R., Hinkley, R.E., and Pierson, G.B. (1975). Tannic-acid stained microtubules with 12, 13, and 15 protofilaments. J. Cell Biol. *65*, 227–233.
3. Tilney, L.G., Bryan, J., Bush, D.J., Fujiwara, K., Mooseker, M.S., Murphy, D.B., and Snyder, D.H. (1973). Microtubules: evidence for 13 protofilaments. J. Cell Biol. *59*, 267–275.
4. Voter, W.A., and Erickson, H.P. (1984). The kinetics of microtubule assembly. J. Biol. Chem. *259*, 10430–10438.
5. Mitchison, T., and Kirschner, M. (1984). Microtubule assembly nucleated by isolated centrosomes. Nature *312*, 232–237.
6. Zheng, Y., Wong, M.L., Alberts, B., and Mitchison, T. (1995). Nucleation of microtubule assembly by a γ-tubulin-containing ring complex. Nature *378*, 578–583.
7. Walker, R.A., O'Brien, E.T., Pryer, N.K., Soboeiro, M.F., Voter, W.A., Erickson, H.P., and Salmon, E.D. (1988). Dynamic instability of individual microtubules analyzed by video light microscopy: rate constants and transition frequencies. J. Cell Biol. *107*, 1437–1448.
8. Hyman, A.A., Salser, S., Drechsel, D.N., Unwin, N., and Mitchison, T.J. (1992). Role of GTP hydrolysis in microtubule dynamics: Information from a slowly hydrolyzable analogue, GMPCPP. Mol. Biol. Cell *3*, 1155–1167.
9. Ruhnow, F., Zwicker, D., and Diez, S. (2011). Tracking single particles and elongated filaments with nanometer precision. Biophys. J. *100*, 2820–2828.
10. Bohner, G., Gustafsson, N., Cade, N.I., Maurer, S.P., Griffin, L.D., and Surrey, T. (2016). Important factors determining the nanoscale tracking precision of dynamic microtubule ends. J. Microsc. *261*, 67–78.
11. Chen, Y., and Hancock, W.O. (2015). Kinesin-5 is a microtubule polymerase. Nat. Commun. *6*, 8160.
12. Mitchison, T., and Kirschner, M. (1984). Dynamic instability of microtubule growth. Nature *312*, 237–242.
13. Duellberg, C., Cade, N.I., Holmes, D., and Surrey, T. (2016). The size of the EB cap determines instantaneous microtubule stability. eLife *5*, e13470.
14. Hill, T.L., and Chen, Y. (1984). Phase changes at the end of a microtubule with a GTP cap. Proc. Natl. Acad. Sci. USA *81*, 5772–5776.
15. Chen, Y., and Hill, T.L. (1985). Monte Carlo study of the GTP cap in a five-start helix model of a microtubule. Proc. Natl. Acad. Sci. USA *82*, 1131–1135.
16. Hill, T.L. (1984). Introductory analysis of the GTP-cap phase-change kinetics at the end of a microtubule. Proc. Natl. Acad. Sci. USA *81*, 6728–6732.
17. Zanic, M., Stear, J.H., Hyman, A.A., and Howard, J. (2009). EB1 recognizes the nucleotide state of tubulin in the microtubule lattice. PLoS One *4*, e7585.

18. Bieling, P., Laan, L., Schek, H., Munteanu, E.L., Sandblad, L., Dogterom, M., Brunner, D., and Surrey, T. (2007). Reconstitution of a microtubule plus-end tracking system in vitro. Nature *450*, 1100–1105.

19. Honnappa, S., Gouveia, S.M., Weisbrich, A., Damberger, F.F., Bhavesh, N.S., Jawhari, H., Grigoriev, I., van Rijssel, F.J.A., Buey, R.M., Lawera, A., *et al*. (2009). An EB1-binding motif acts as a microtubule tip localization signal. Cell *138*, 366–376.

20. Maurer, S.P., Cade, N.I., Bohner, G., Gustafsson, N., Boutant, E., and Surrey, T. (2014). EB1 accelerates two conformational transitions important for microtubule maturation and dynamics. Curr. Biol. *24*, 372–384.

21. Rickman, J., Duellberg, C., Cade, N.I., Griffin, L.D., and Surrey, T. (2017). Steady-state EB cap size fluctuations are determined by stochastic microtubule growth and maturation. Proc. Natl. Acad. Sci. USA *114*, 3427–3432.

22. VanBuren, V., Odde, D.J., and Cassimeris, L. (2002). Estimates of lateral and longitudinal bond energies within the microtubule lattice. Proc. Natl. Acad. Sci. USA *99*, 6035–6040.

23. VanBuren, V., Cassimeris, L., and Odde, D.J. (2005). Mechanochemical model of microtubule structure and self-assembly kinetics. Biophys. J. *89*, 2911–2926.

24. Gardner, M.K., Charlebois, B.D., Jánosi, I.M., Howard, J., Hunt, A.J., and Odde, D.J. (2011). Rapid microtubule self-assembly kinetics. Cell *146*, 582–592.

25. Zakharov, P., Gudimchuk, N., Voevodin, V., Tikhonravov, A., Ataullakhanov, F.I., and Grishchuk, E.L. (2015). Molecular and mechanical causes of microtubule catastrophe and aging. Biophys. J. *109*, 2574–2591.

26. Piedra, F.A., Kim, T., Garza, E.S., Geyer, E.A., Burns, A., Ye, X., and Rice, L.M. (2016). GDP-to-GTP exchange on the microtubule end can contribute to the frequency of catastrophe. Mol. Biol. Cell *27*, 3515–3525.

27. Jonasson, E.M., Mauro, A.J., Li, C., Labuza, E.C., Mahserejian, S.M., Scripture, J.P., Gregoretti, I.V., Alber, M., and Goodson, H.V. (2020). Behaviors of individual microtubules and microtubule populations relative to critical concentrations: dynamic instability occurs when critical concentrations are driven apart by nucleotide hydrolysis. Mol. Biol. Cell *31*, 589–618.

28. Manka, S.W., and Moores, C.A. (2018). The role of tubulin–tubulin lattice contacts in the mechanism of microtubule dynamic instability. Nat. Struct. Mol. Biol. *25*, 607–615.

29. Alushin, G.M., Lander, G.C., Kellogg, E.H., Zhang, R., Baker, D., and Nogales, E. (2014). High-resolution microtubule structures reveal the structural transitions in αβ-tubulin upon GTP hydrolysis. Cell *157*, 1117–1129.

30. Wang, Z., and Sheetz, M.P. (2000). The C-terminus of tubulin increases cytoplasmic dynein and kinesin processivity. Biophys. J. *78*, 1955–1964.

31. White, S.R., Evans, K.J., Lary, J., Cole, J.L., and Lauring, B. (2007). Recognition of C-terminal amino acids in tubulin by pore loops in spastin is important for microtubule severing. J. Cell Biol. *176*, 995–1005.

32. Nithianantham, S., Le, S., Seto, E., Jia, W., Leary, J., Corbett, K.D., Moore, J.K., and Al-Bassam, J. (2015). Tubulin cofactors and Arl2 are cage-like chaperones that regulate the soluble αβ-tubulin pool for microtubule dynamics. eLife *4*, e08811.

33. Montecinos-Franjola, F., Schuck, P., and Sackett, D.L. (2016). Tubulin dimer reversible dissociation: affinity, kinetics, and demonstration of a stable monomer. J. Biol. Chem. *291*, 9281–9294.

34. Mitchison, T.J. (1993). Localization of an exchangeable GTP binding site at the plus end. Science *261*, 1044–1047.

35. Löwe, J., Li, H., Downing, K.H., and Nogales, E. (2001). Refined structure of αβ-tubulin at 3.5 Å resolution. J. Mol. Biol. *313*, 1045–1057.

36. David-Pfeuty, T., Erickson, H.P., and Pantaloni, D. (1977). Guanosinetriphosphatase activity of tubulin associated with microtubule assembly. Proc. Natl. Acad. Sci. USA *74*, 5372–5376.

37. Davis, A., Sage, C.R., Dougherty, C.A., and Farrell, K.W. (1994). Microtubule dynamics modulated by guanosine triphosphate hydrolysis activity of β-tubulin. Science *264*, 839–842.

38. Kikkawa, M., Ishikawa, T., Nakata, T., Wakabayashi, T., and Hirokawa, N. (1994). Direct visualization of the microtubule lattice seam both in vitro and in vivo. J. Cell Biol. *127*, 1965–1971.

39. Ti, S.C., Alushin, G.M., and Kapoor, T.M. (2018). Human β-tubulin isotypes can regulate microtubule protofilament number and stability. Dev. Cell *47*, 175–190.

40. Nogales, E., Whittaker, M., Milligan, R.A., and Downing, K.H. (1999). High-resolution model of the microtubule. Cell *96*, 79–88.

41. Chaaban, S., Jariwala, S., Hsu, C.T., Redemann, S., Kollman, J.M., Müller-Reichert, T., Sept, D., Bui, K.H., and Brouhard, G.J. (2018). The structure and dynamics of C. elegans tubulin reveals the mechanistic basis of microtubule growth. Dev. Cell *47*, 191–204.e8.

42. Katsuki, M., Drummond, D.R., and Cross, R.A. (2014). Ectopic A-lattice seams destabilize microtubules. Nat. Commun. *5*, 3094.

43. Gudimchuk, N.B., Ulyanov, E.V., O'Toole, E., Page, C.L., Vinogradov, D.S., Morgan, G., Li, G., Moore, J.K., Szczesna, E., Roll-Mecak, A., *et al*. (2020). Mechanisms of microtubule dynamics and force generation examined with computational modeling and electron cryotomography. Nat. Commun. *11*, 3765.

44. Kim, T., and Rice, L.M. (2019). Long-range, through-lattice coupling improves predictions of microtubule catastrophe. Mol. Biol. Cell *30*, 1451–1462.

45. Mickolajczyk, K.J., Geyer, E.A., Kim, T., Rice, L.M., and Hancock, W.O. (2019). Direct observation of individual tubulin dimers binding to growing microtubules. Proc. Natl. Acad. Sci. USA *116*, 7314–7322.

46. Schaedel, L., Triclin, S., Chrétien, D., Abrieu, A., Aumeier, C., Gaillard, J., Blanchoin, L., Théry, M., and John, K. (2019). Lattice defects induce microtubule self-renewal. Nat. Phys. *15*, 830–838.

47. Schaedel, L., John, K., Gaillard, J., Nachury, M.V., Blanchoin, L., and Thery, M. (2015). Microtubules self-repair in response to mechanical stress. Nat. Mater. *14*, 1156–1163.

48. Aumeier, C., Schaedel, L., Gaillard, J., John, K., Blanchoin, L., and Théry, M. (2016). Self-repair promotes microtubule rescue. Nat. Cell Biol. *18*, 1054–1064.

49. Mozziconacci, J., Sandbland, L., Wachsmuth, M., Brunner, D., and Karsenti, E. (2008). Tubulin dimers oligomerize before their incorporation into microtubules. PLoS One *3*, e3821.

50. Ayaz, P., Munyoki, S., Geyer, E.A., Piedra, F.A., Vu, E.S., Bromberg, R., Otwinowski, Z., Grishin, N.V., Brautigam, C.A., and Rice, L.M. (2014). A tethered delivery mechanism explains the catalytic action of a microtubule polymerase. eLife *3*, e03069.

51. Chrétien, D., Fuller, S.D., and Karsenti, E. (1995). Structure of growing microtubule ends: two-dimensional sheets close into tubes at variable rates. J. Cell Biol. *129*, 1311–1328.

52. Coombes, C.E., Yamamoto, A., Kenzie, M.R., Odde, D.J., and Gardner, M.K. (2013). Evolving tip structures can explain age-dependent microtubule catastrophe. Curr. Biol. *23*, 1342–1348.

53. Demchouk, A.O., Gardner, M.K., and Odde, D.J. (2011). Microtubule tip tracking and tip structures at the nanometer scale using digital fluorescence microscopy. Cell. Mol. Bioeng. *4*, 192–204.

54. Chen, G.Y., Cleary, J.M., Asenjo, A.B., Chen, Y., Mascaro, J.A., Arginteanu, D.F.J., Sosa, H., and Hancock, W.O. (2019). Kinesin-5 promotes microtubule nucleation and assembly by stabilizing a lattice-competent conformation of tubulin. Curr. Biol. *29*, 2259–2269.

55. Aher, A., Rai, D., Schaedel, L., Gaillard, J., John, K., Liu, Q., Altelaar, M., Blanchoin, L., Thery, M., and Akhmanova, A. (2020). CLASP mediates microtubule repair by restricting lattice damage and regulating tubulin incorporation. Curr. Biol. *30*, 2175–2183.

56. Mahamdeh, M., Simmert, S., Luchniak, A., Schäffer, E., and Howard, J. (2018). Label-free high-speed wide-field imaging of single microtubules using interference reflection microscopy. J. Microsc. *272*, 60–66.

57. Andrecka, J., Ortega Arroyo, J., Lewis, K., Cross, R.A., and Kukura, P. (2016). Label-free imaging of microtubules with sub-nm precision using interferometric scattering microscopy. Biophys. J. *110*, 214–217.

58. Young, G., Hundt, N., Cole, D., Fineberg, A., Andrecka, J., Tyler, A., Olerinyova, A., Ansari, A., Marklund, E.G., Collier, M.P., *et al*. (2018). Quantitative mass imaging of single molecules in solution. Science *360*, 423–427.

59. Wieczorek, M., Bechstedt, S., Chaaban, S., and Brouhard, G.J. (2015). Microtubule-associated proteins control the kinetics of microtubule nucleation. Nat. Cell Biol. *17*, 907–916.

60. Thawani, A., Rale, M.J., Coudray, N., Bhabha, G., Stone, H.A., Shaevitz, J.W., and Petry, S. (2020). The transition state and regulation of γ-TuRC-mediated microtubule nucleation revealed by single molecule microscopy. eLife *9*, e54253.

61. Kerssemakers, J.W.J., Munteanu, E.L., Laan, L., Noetzel, T.L., Janson, M.E., and Dogterom, M. (2006). Assembly dynamics of microtubules at molecular resolution. Nature *442*, 709–712.

62. Schek III, H.T., Gardner, M.K., Cheng, J., Odde, D.J., and Hunt, A.J. (2007). Microtubule assembly dynamics at the nanoscale. Curr. Biol. *17*, 1445–1455.

63. Castle, B.T., and Odde, D.J. (2013). Brownian dynamics of subunit addition-loss kinetics and thermodynamics in linear polymer self-assembly. Biophys. J. *105*, 2528–2540.

64. Geyer, E.A., Miller, M.P., Brautigam, C.A., Biggins, S., and Rice, L.M. (2018). Design principles of a microtubule polymerase. eLife *7*, e34574.

65. Johnson, V., Ayaz, P., Huddleston, P., and Rice, L.M. (2011). Design, overexpression, and purification of polymerization-blocked yeast αβ-tubulin mutants. Biochemistry *50*, 8636–8864.

66. Mandelkow, E., Mandelkow, E., and Milligan, R.A. (1991). Microtubule dynamics and microtubule caps: a time-resolved cryo-electron microscopy study. J. Cell Biol. *114*, 977–991.

67. Wang, H.W., and Nogales, E. (2005). Nucleotide-dependent bending flexibility of tubulin regulates microtubule assembly. Nature *435*, 911–915.

68. Nawrotek, A., Knossow, M., and Gigant, B. (2011). The determinants that Govern microtubule assembly from the atomic structure of GTP-tubulin. J. Mol. Biol. *412*, 35–42.

69. Rice, L.M., Montabana, E.A., and Agard, D.A. (2008). The lattice as allosteric effector: structural studies of αβ- and γ-tubulin clarify the role of GTP in microtubule assembly. Proc. Natl. Acad. Sci. USA *105*, 5378–5383.

70. McIntosh, J.R., O'Toole, E., Morgan, G., Austin, J., Ulyanov, E., Ataullakhanov, F., and Gudimchuk, N. (2018). Microtubules grow by the addition of bent guanosine triphosphate tubulin to the tips of curved protofilaments. J. Cell Biol. *217*, 2691–2708.

71. Atherton, J., Jiang, K., Stangier, M.M., Luo, Y., Hua, S., Houben, K., Hoff, J.J.E. Van, Joseph, A., Scarabelli, G., Grant, B.J., *et al*. (2017). A structural model for microtubule minus-end recognition and protection by CAMSAP proteins. Nat. Struct. Mol. Biol. *24*, 931–943.

72. Atherton, J., Stouffer, M., Francis, F., and Moores, C.A. (2018). Microtubule architecture in vitro and in cells revealed by cryo-electron tomography. Acta Cryst. *D74*, 572–584.

73. Guesdon, A., Bazile, F., Buey, R.M., Mohan, R., Monier, S., García, R.R., Angevin, M., Heichette, C., Wieneke, R., Tampé, R., *et al*. (2016). EB1 interacts with outwardly curved and straight regions of the microtubule lattice. Nat. Cell Biol. *18*, 1102–1108.

74. McIntosh, J.R., O'Toole, E., Page, C., and Morgan, G. (2020). Ultrastructural analysis of microtubule ends. In Cytoskeleton Dynamics: Methods and Protocols, H. Maiato, ed. (Springer USA), pp. 191–209.

75. Rice, L.M. (2018). A new look for the growing microtubule end? J. Cell Biol. *217*, 2609–2611.

76. Erickson, H.P. (2019). Microtubule assembly from single flared protofilaments - forget the cozy corner? Biophys. J. *116*, 2240–2245.

77. Alberts, B., Johnson, A., Lewis, J., Raff, M., Roberts, K., and Walter, P. (2002). Molecular Biology of the Cell, 4th Edition (Garland).

78. Nogales, E., and Wang, H. (2006). Structural intermediates in microtubule assembly and disassembly: how and why? Curr. Opin. Cell Biol. *18*, 179–184.

79. Knossow, M., Campanacci, V., Khodja, L.A., and Gigant, B. (2020). The mechanism of tubulin assembly into microtubules: insights from structural studies. iScience *23*, 101511.

80. Estévez-Gallego, J., Josa-Prado, F., Ku, S., Buey, R.M., Balaguer, F.A., Prota, A.E., Lucena-Agell, D., Kamma-Lorger, C., Yagi, T., Iwamoto, H., *et al*. (2020). Structural model for differential cap maturation at growing microtubule ends. eLife *9*, e50155.

81. Bowne-Anderson, H., Zanic, M., Kauer, M., and Howard, J. (2013). Microtubule dynamic instability: A new model with coupled GTP hydrolysis and multistep catastrophe. BioEssays *35*, 452–461.

82. Roostalu, J., Thomas, C., Cade, N.I., Kunzelmann, S., Taylor, I.A., and Surrey, T. (2020). The speed of GTP hydrolysis determines GTP cap size and controls microtubule stability. eLife *9*, e51992.

83. Keller, P.J., Pampaloni, F., and Stelzer, E.H.K. (2007). Three-dimensional preparation and imaging reveal intrinsic microtubule properties. Nat. Methods *4*, 843–846.

84. Rai, A., Liu, T., Glauser, S., Katrukha, E.A., Estévez-Gallego, J., Rodríguez-García, R., Fang, W.S., Díaz, J.F., Steinmetz, M.O., Altmann, K.H., *et al*. (2020). Taxanes convert regions of perturbed microtubule growth into rescue sites. Nat. Mater. *19*, 355–365.

85. Strothman, C., Farmer, V., Arpag, G., Rodgers, N., Podolski, M., Norris, S., Ohi, R., and Zanic, M. (2019). Microtubule minus-end stability is dictated by the tubulin off-rate. J. Cell Biol. *218*, 2841–2853.

86. Hyman, A.A., Chretien, D., Arnal, I., and Wade, R.H. (1995). Structural changes accompanying GTP hydrolysis in microtubules: information from a slowly hydrolyzable analogue guanylyl-(α,β)-methylene-diphosphonate. J. Cell Biol. *128*, 117–125.

87. Peet, D.R., Burroughs, N.J., and Cross, R.A. (2018). Kinesin expands and stabilizes the GDP-microtubule lattice. Nat. Nanotechnol. *13*, 386–391.

88. Shima, T., Morikawa, M., Kaneshiro, J., Kambara, T., Kamimura, S., Yagi, T., Iwamoto, H., Uemura, S., Shigematsu, H., Shirouzu, M., *et al*. (2018). Kinesin-binding–triggered conformation switching of microtubules contributes to polarized transport. J. Cell Biol. *217*, 4164–4183.

89. Zhang, R., Lafrance, B., and Nogales, E. (2018). Separating the effects of nucleotide and EB binding on microtubule structure. Proc. Natl. Acad. Sci. USA *115*, 6191–6200.

90. Brouhard, G.J., and Rice, L.M. (2018). Microtubule dynamics: an interplay of biochemistry and mechanics. Nat. Rev. Mol. Cell Biol. *19*, 451–463.

91. Debs, G.E., Cha, M., Liu, X., Huehn, A.R., and Sindelar, C.V. (2020). Dynamic and asymmetric fluctuations in the microtubule wall captured by high-resolution cryoelectron microscopy. Proc. Natl. Acad. Sci. USA *117*, 16976–16984.

92. Chretien, D., and Fuller, S.D. (2000). Microtubules switch occasionally into unfavorable configurations during elongation. J. Mol. Biol. *298*, 663–676.

93. Hunyadi, V., Chretien, D., and Janosi, I.M. (2005). Mechanical stress induced mechanism of microtubule catastrophes. J. Mol. Biol. *348*, 927–938.

94. Bowne-Anderson, H., Hibbel, A., and Howard, J. (2015). Regulation of microtubule growth and catastrophe: unifying theory and experiment. Trends Cell Biol. *25*, 769–779.

95. Akhmanova, A., and Hoogenraad, C.C. (2015). Microtubule minus-end-targeting proteins. Curr. Biol. *25*, R162–R171.

96. Hendershott, M.C., and Vale, R.D. (2014). Regulation of microtubule minus-end dynamics by CAMSAPs and Patronin. Proc. Natl. Acad. Sci. USA *111*, 5860–5865.

97. Bechstedt, S., Lu, K., and Brouhard, G.J. (2014). Doublecortin recognizes the longitudinal curvature of the microtubule end and lattice. Curr. Biol. *24*, 2366–2375.

98. Al-Bassam, J., Kim, H., Brouhard, G., van Oijen, A., Harrison, S.C., and Chang, F. (2010). CLASP promotes microtubule rescue by recruiting tubulin dimers to the microtubule. Dev. Cell *19*, 245–258.

99. Kuo, Y., Trottier, O., Mahamdeh, M., and Howard, J. (2019). Spastin is a dual-function enzyme that severs microtubules and promotes their regrowth to increase the number and mass of microtubules. Proc. Natl. Acad. Sci. USA *116*, 5533–5541.

100. Sharp, D.J., and Ross, J.L. (2012). Microtubule-severing enzymes at the cutting edge. J. Cell Sci. *125*, 2561–2569.

101. Vemu, A., Szczesna, E., Zehr, E.A., Spector, J.O., Grigorieff, N., Deaconescu, A.M., and Roll-mecak, A. (2018). Severing enzymes amplify microtubule arrays through lattice GTP-tubulin incorporation. Science *361*, eaau1504.

102. Sandate, C.R., Szyk, A., Zehr, E.A., Lander, G.C., and Roll-Mecak, A. (2019). An allosteric network in spastin couples multiple activities required for microtubule severing. Nat. Struct. Mol. Biol. *26*, 671–678.

103. Triclin, S., Inoue, D., Gaillard, J., Htet, Z.M., DeSantis, M.E., Portran, D., Derivery, E., Aumeier, C., Schaedel, L., John, K., *et al*. (2021). Self-repair protects microtubules from destruction by molecular motors. Nat. Mater. https://doi.org/10.1038/s41563-020-00905-0.

104. de Forges, H., Pilon, A., Cantaloube, I., Pallandre, A., Haghiri-Gosnet, A.M., Perez, F., and Poüs, C. (2016). Localized mechanical stress promotes microtubule rescue. Curr. Biol. *26*, 3399–3406.

105. Bollinger, J.A., Imam, Z.I., Stevens, M.J., and Bachand, G.D. (2020). Tubulin islands containing slowly hydrolyzable GTP analogs regulate the mechanism and kinetics of microtubule depolymerization. Sci. Rep. *10*, 13661.

106. Panda, D., Miller, H.P., Banjeree, A., Luduena, R.F., and Wilson, L. (1994). Microtubule dynamics in vitro are regulated by the tubulin isotype composition. Proc. Natl. Acad. Sci. USA *91*, 11358–11362.

107. Sullivan, K.F. (1988). Structure and utilization of tubulin isotypes. Annu. Rev. Cell Biol. *4*, 687–716.

108. Vemu, A., Atherton, J., Spector, J.O., Moores, C.A., and Roll-Mecak, A. (2017). Tubulin isoform composition tunes microtubule dynamics. Mol. Biol. Cell *28*, 3564–3572.

109. Roll-Mecak, A. (2020). The tubulin code in microtubule dynamics and information encoding. Dev. Cell *54*, 7–20.

110. Chakraborti, S., Natarajan, K., Curiel, J., Janke, C., and Liu, J. (2016). The emerging role of the tubulin code: from the tubulin molecule to neuronal function and disease. Cytoskeleton *73*, 521–550.

111. Janke, C., and Magiera, M.M. (2020). The tubulin code and its role in controlling microtubule properties and functions. Nat. Rev. Mol. Cell Biol. *21*, 307–326.

112. Margolin, G., Gregoretti, I.V., Cickovski, T.M., Li, C., Shi, W., and Mogilner, A. (2012). The mechanisms of microtubule catastrophe and rescue: implications from analysis of a dimer-scale computational model. Mol. Biol. Cell *23*, 642–656.